ALL-COPPER CHIP-TO-SUBSTRATE INTERCONNECTIONS FOR FLIP-CHIP PACKAGES

A Thesis
Presented to
The Academic Faculty

by

Charles Hunter Lightsey

In Partial Fulfillment
of the Requirements for the Degree
Master of Science in the
School of Chemical and Biomolecular Engineering

Georgia Institute of Technology
May of 2010

ALL-COPPER CHIP-TO-SUBSTRATE INTERCONNECTIONS FOR FLIP-CHIP PACKAGES

Approved by:

Dr. Paul A. Kohl, Advisor
School of Chemical and Biomolocular Engineering
Georgia Institute of Technology

Dr. Dennis W. Hess
School of Chemical and Biomolecular Engineering
Georgia Institute of Technology

Dr. Peter J. Hesketh
School of Mechanical Engineering
Georgia Institute of Technology

Date Approved:

In dedication to my parents April and Dale Lightsey.

ACKNOWLEDGEMENTS

I would like to first thank my advisor, Dr. Paul Kohl, for all of his guidance and discussion that allowed me to succeed in my graduate studies at Georgia Institute of Technology. He has not only aided in my development as a researcher, but he has educated me on valuable topics such as leadership, planning, honor and reliability. I would especially like to thank Dr. Dennis W. Hess and Dr. Peter J. Hesketh for participating in my thesis committee. They have provided me with profound insight concerning my graduate research. I would like to thank Daphne Perry her general support and aid concerning lab necessities, travel assistance, and group planning. Also, I would like to extend a special thanks to the supporters of my research, the Semiconductor Research Consortium and National Semiconductor, and the corresponding industrial mentors involved with this project through the SRC.

I have thoroughly enjoyed my interactions with all of the members of the Kohl research group during my time at Georgia Tech. I would have never succeeded without their tremendous support and advice concerning my experimentation and analysis. Tyler Osborn, especially, provided an exorbitant amount of guidance during my initial time at Georgia Tech. A special thanks is due to Dr. Hyo-Chol Koo and Ping An for the many discussions, assistance, interactions concerning my research. Thank you also to Venmathy Rajarathinam, Nathan Fritz, and Mehrsa Raeiszadeh.

Finally and most importantly, I would like to thank my parents (April and Dale Lightsey), my sister (Sara-Claire Lightsey), and my girlfriend (Dinah Dupont) for all their love and support.

TABLE OF CONTENTS

LIST OF FIGURES AND TABLES

CHAPTER 1

INTRODUCTION

1.1 Introduction to Flip-Chip Packaging

Digital electronic device performance doubles about every two years primarily due to the shrinkage of transistors, as described by Moore's Law. In 1965, Gordon E. Moore correctly predicted that the number of transistors per integrated circuit would double every two years while the cost of production would simultaneously decrease.[1] His prediction has been fulfilled over the past 40 years. Since the transistor density and chip size have increased following Moore's initial conjecture, ever increasing demands have been placed on the packaging (i.e. protection and electrical connection) of integrated circuits. According to the 2007 International Technology Roadmap for Semiconductors, "packaging is now the limiting factor in cost and performance for many types of devices."

The flip-chip package is the preferred package for high-performance devices such as micro-processors. This type of package allows for mechanical and electrical connections between the chip and substrate over an area array on the active surface of the chip, allowing for a high number of connections to be made. Solder is the preferred method for making high performance mechanical and electrical flip-chip connections in a flip chip package (i.e. first-level packaging), but this process is not without limitations. One of the weaknesses with solder ball connections is that the aspect ratio (height-to-width) can cause chip-to-substrate offset problems for fine-pitch, input-output (I/O) connections. Recently, solder-capped copper pillars have mitigated the aspect ratio concerns by providing chip-to-substrate offsets greater than the height of the solder cap.

Solder-capped, copper pillars also have the benefit of moving the location of the brittle copper-tin intermetallic from the chip surface to the pillar structure.[2] Copper-tin intermetallics formed at the solder-to-copper interface decrease the thermomechanical reliability of the connection. Lead or other metals (e.g. silver-copper) are added to tin to increase the tensile and shear strength and to lower the melting point of the solder. Lead is an environmental toxin, and lead-free packaging solutions are preferred. The use and distribution of underfill material, which is required for thermomechanical reliability in the flip-chip solder system, introduces additional problems especially as the gap between the chip and the substrate decreases. In addition to the mechanical limitations, solder has a high electrical resistance and parasitic capacitance due to the presence of underfill materials. Solder also has a low electromigration resistance, which is exacerbated by the higher DC power requirements.

1.2 Replacing Solder with All-Copper Interconnects

Flip-chip, all-copper connections between the chip and substrate eliminate many of the electrical and mechanical problems with solder, as stated above. Copper has superior electrical conductivity and electromigration resistance. Instead of using underfill in this system, a polymer collar can be used as an electroplating mold and a mechanical support. With the elimination of underfill, the quality of the signal transmitted through an interconnect is improved by decreasing the permittivity and loss, and the fabrication process is potentially simplified. Since the yield stress and Young's modulus are higher for copper than solder, copper is different than solder and superior in terms of yield. By removing tin from the package, the brittle intermetallics are not formed. Unlike the solder ball, the all-copper interconnect is not limited by aspect ratio.

Finally, the elimination of solder, underbump metallurgy, and stripping chemicals makes the all-copper interconnect system environmentally friendly.

Previously, a novel method for bonding two copper pillars by forming an all-copper fillet via electroless deposition and an annealing step was reported.[3-5] This novel all-copper bonding method can be used for I/O connections at first-level package. Copper is inexpensive and extreme processing conditions (i.e. high pressure, atomically clean surfaces, high temperature, etc.) are not required. Various other methods of copper bonding require the use of extreme processing conditions, and are not able to compensate for x-y-z offset.[6-7] Since electroless copper bonding has been shown to compensate for offset in all directions, this bonding method is an interesting alternative to solder.

1.3 Research Objectives

An initial goal in this work was to optimize the processing conditions used to make the polymer collar by analyzing the optical properties of the photosensitive polymer Avatrel 8000P. Avatrel 8000P, shown in Figure 1, consists of a norbornene backbone with fluorinated alcohol groups which provide solubility in an aqueous base and carboxylic acid groups which provide cross-linking sites with epoxy units. The polymer formulation is a mixture containing a multifunctional epoxy cross-linker, a photo-catalyst, and an adhesion promoter. Avatrel 8000P is an ideal candidate for the polymer collar due to ease of processing, relatively high elastic modulus, and capability of high aspect ratios.[8] The optical properties were studied and compared to Avatrel 2000P and SU-8 to better understand the high aspect ratio of the patterned films and to optimize the processing conditions.

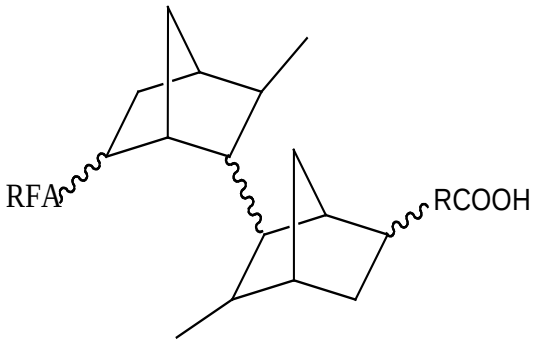

Figure 1. The chemical structure of Avatrel 8000P (RFA = hydroxyl(polyfluoro)alkyl).

The main scope of this study is to evaluate the electroless bond formed between two copper surfaces and the affect of annealing on the bond. The post-plating anneal can strengthen the electroless copper joint by initiating grain growth, removing defects, and reducing the amount of entrapped hydrogen. Crack initiation and propagation can occur at defects, such as seams and voids, in the electroless bond. Understanding the affect of annealing conditions on the defects present is important to improving the process and minimizing the thermal excursions. Grain growth in the electroless bonded region implies an increase in ductility, yielding a more thermomechanically compliant I/O. Finding the minimum annealing temperature is important because the zero-stress temperature of the deposited copper is dependent on the annealing temperature. By lowering the zero-stress temperature of the copper, the thermomechanical stress, due to a mismatch in the coefficient of thermal expansion between the silicon chip and substrate, is lowered. A lower anneal temperature will also minimize the degradation of the mechanical properties or an organic substrate, such as FR-4 grade printed circuit board.

In a previous report, Osborn et al. improved the electroless bath by increasing the plating rate through an increase in bath temperature. Polyethylene glycol was added as a

surface inhibitor and surfactant to moderate the plating rate and promote deposition in spatially restricted regions. The oxidation of formaldehyde produces hydrogen which can result in hydrogen bubble entrapment. Previously, steps were taken to lower the hydrogen entrapment and produce a mechanically compliant, all-copper bond in a 2 to 4 hours process, compared to the original 18 hour cycle.[5] However, the bath used by Osborn et al. contained proprietary additives and an organic surface agent, polyethylene glycol. The incorporation of organic additives in electroless baths can affect the electrical and mechanical film properties in a variety of complex ways.[9-11] In this work, the electroless bonding of two copper surfaces has been achieved, over large and small standoff distances between copper surfaces, by using a standard alkaline electroless copper bath containing a minimal amount of organic additives.

CHAPTER 2

EXPERIMENTAL METHODS AND TECHNIQUES

2.1 Fabrication of All-Copper Test Structures

The test structures were fabricated on 100 mm diameter, p-type silicon wafers with a <100> orientation. Pillar fabrication was performed at wafer level similar to a previously described process.[3] A 1μm-thick SiO_2 layer was grown by thermal oxidation. Metallization layers, consisting of chromium/copper/titanium (Cr/Cu/Ti), were deposited in a CVC (Rochester, NY) DC sputterer with thicknesses of 30 nm, 300 nm, and 20 nm, respectively. A 1.5 μm-thick SiO_2 layer was grown on the Ti layer by chemical vapor deposition (CVD) in a Unaxis (St. Petersburg, FL) PECVD at 250^{o}C. Microposit SC1813 photoresist (Rohm and Haas, Philadelphia, PA) and buffered oxide etch of the underlying SiO_2 and Ti layers were used to pattern the pillars. The remaining photoresist was stripped with acetone. At this point in processing, pillarless test structures (i.e. copper pads) are fabricated, and these samples can be used to assess electroless bonding between two copper surfaces with a large standoff distance. To create a standoff distance between the pads of two flip-chip aligned samples, (Polyscience Inc., Warrington, PA) polystyrene microspheres with a diameter of 117.5 ± 2.6 μm were placed between the two aligned parts. A diagram of the system is shown in Figure 2B. Pillared samples were fabricated in the manner described below.

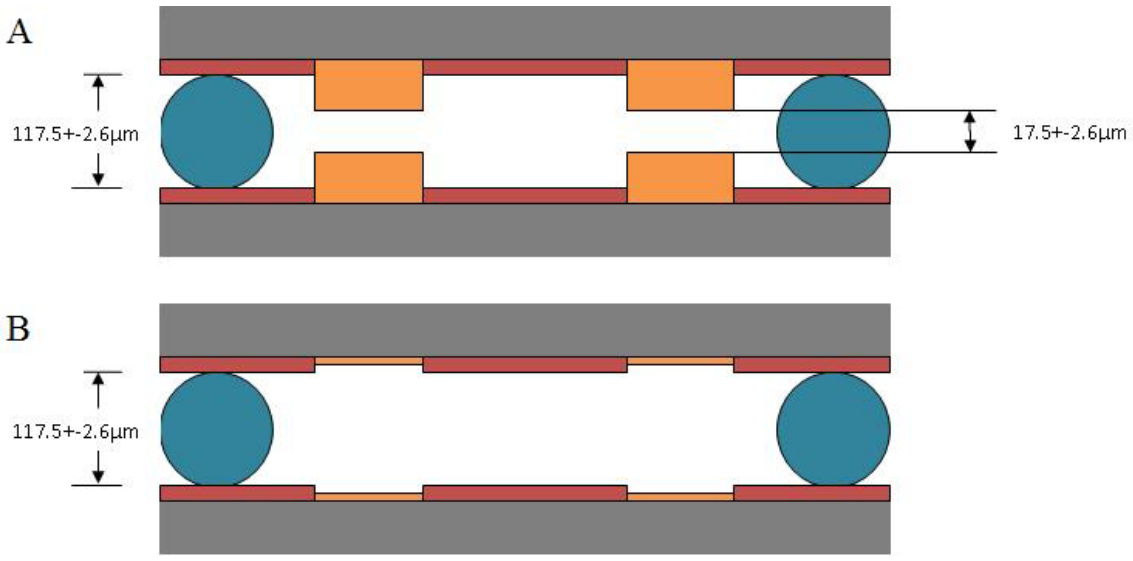

Figure 2. A diagram of the aligned test structures for the pillar-to-pillar system (A) and the pad-to-pad system (B).

A novel negative-tone photoresist, Avatrel 8000P (Promerus LLC, Brecksville, OH), was used to create the electroplating mold for the copper pillars.[12] Avatrel 8000P was spun on the wafer at 900 RPM in order to give a film thickness of 45-50 µm. The film was soft baked on a hot plate for 5 minutes at 100^{o}C, followed by ultraviolet exposed, 365 nm wavelength, at a dose of 500 mJ/cm^{2}. The film was then post-exposure baked for 5 minutes at 100^{o}C, and developed in MF-319 for 8 minutes. The mask used for photolithography was composed of an array of annular circles (inside diameter was 300 µm) and annual squares (inside dimension was 150µm). A diagram of the mask layout is shown in Figure 3. Next, copper pillars were grown inside the polymer mold via electrodeposition at a current density of 10-15 mA/cm^{2} and in an electrolyte which is described in Table 1. After plating, the polymer collars were stripped in a highly alkaline solution of potassium hydroxide at 80^{o}C to ensure polymer contamination does not

interfere with experimental results. The wafers were then pre-annealed at 250°C for 1. Finally, the wafers were diced into rectangular samples with dimensions of 1.5x1.5 cm.

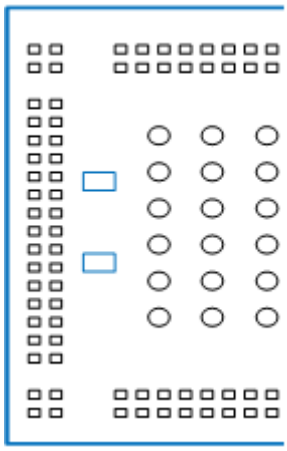

Figure 3. A diagram of interconnect location on the chip/mask.

To create a standoff distance between the pillars of two flip-chip aligned samples, (Polyscience Inc., Warrington, PA) polystyrene microspheres with a diameter of 117.5 ± 2.6 µm were placed between the two aligned parts. A diagram of the system is shown in Figure 2B. Organic additives incorporated in the outer layers, or at the surface of the copper pillars were removed by first oxidizing the copper in a hydrogen peroxide solution (2-3 minutes) and followed by dissolving the oxide in dilute sulfuric acid solution (2-3 minutes), as described by Stangl et al.[13] The pillars were bonded via electroless copper deposition in an electrolyte described in Table 1. Continuous air purging was used during electroless deposition and bonding in order to stabilize the bath. The open surface deposition rate of the electroless bath was 10 µm/hr. All samples were electrolessly plated for 4 hours and the initial standoff distance between two aligned pillars was 10-15 µm depending on pillar surface roughness and the diameters of the polystyrene

microspheres. The macroscopic surface roughness of the pillars before electroless plating was from 3-5 μm.

Table 1. A description of the electroless and electroplating baths.

	Electroplating Bath	**Electroless Plating Bath**
Components	H_2SO_4 (180 g/L)	$CuSO_4 \cdot 5H_2O$ (18 g/L)
	$CuSO_4 \cdot 5H_2O$ (80 g/L)	Ethylenediaminetetraacetic Acid (48 g/L)
	Polyethylene Glycol (600 ppm)	KOH (49.4 g/L)
	bis-(Sodium Sulfopropyl)-disulfide (0.2 g/L)	Paraformaldehyde (8.95 g/L)
	HCl (100 ppm)	$K_4Fe(CN)_6$ (60 mg/L)
		HCl (1 mL/L)
Temperature	25°C	60°C
pH	< 1	13
Agitation	Moderate	Moderate

Pillar annealing was performed in a horizontal tube furnace, under nitrogen environment, for 1 hour. The bond strength was calculated from shear testing experiments. These experiments were performed by fixing one chip and applying a load to the other chip in an Instron 5842 (Norwood, MA). A constant shear rate of 10 μm/min was employed. Surface morphology and bonding microstructure was examined with an FEI Nova Nanolab 200 (Hillsboro, OR) focused ion beam/scanning electron microscope (FIB/SEM).

2.2 Photopolymer Characterization Techniques

Avatrel 2000P was processed according to the procedures of Bai et al.[14-15] and SU-8 was processed according to the procedures listed on the MicroChem website.[16] Avatrel 8000P samples were spin coated onto <100> silicon wafers and then soft-baked on a hotplate at 100ºC for 5 minutes to remove the solvent from the polymer film. A variable density optical mask (Opto-line International Inc.) was used to study the effect of dose on polymer properties. A 1 kW Hg-Xe lamp with 365 nm filter was used for UV exposure, and the post exposure bake was performed on a hotplate at 100ºC for 5 minutes. The Avatrel 8000P films were developed in MF-319 (Shipley) which contained tetramethylammonium hydroxide (TMAH) and a surfactant. Curing was performed in a nitrogen purged furnace, and the samples were ramped to their cure temperature at 5ºC/min and held at temperature for 1 hour. The furnace was allowed to cool slowly by natural convection to room temperature.

A Zeiss Ultra 60 was used to obtain scanning electron microscope (SEM) images of the processed films. Film thicknesses were measured with a Veeco Dektak profilometer, and UV absorption was measured on quartz wafers with a Hewlett Packard 8543 UV-vis spectrophotometer. The residual film stress in polymer films was measured at room temperature using the Flexus Tencor F2320. Weight loss due to temperature exposure was measured using a TA Instruments Q50 thermogravimetric analyzer (TGA). The temperature inside the sample chamber was increased at a rate of 5^{o}C/min or $.5^{o}$C/min f The contrast (γ) of the photosensitive polymer was obtained by measuring film thickness after developing as a function of exposure dose.

The contrast (γ) of the photosensitive polymer was obtained by measuring film thickness after developing as a function of exposure dose. Equation 1 describes the relationship between exposure dose and contrast:

$$\gamma = \frac{1}{\log_{10}\left(\frac{D_{100}}{D_0}\right)} \quad [1]$$

D_{100} is the exposure dose at which none of the photodefined material is removed upon exposure to developer, and D_0 is the exposure dose at which all of the photodefined material is removed. Mathematically γ represents the slope of the linear region of a plot of normalized film thickness versus the log of exposure dose.

CHAPTER 3

PROCESS OPTIMIZATION

3.1 Electroless Bath Simplification

In previous works, Osborn et al. used a commercially available electroless bath, Circuposit 3350 (Rohm and Haas).[3, 5] However, additives and impurities in commercial baths can change, or are at least outside the control of the experimenter, which complicates the electroless experiments. Additives which may assist the regular use of electroless baths, such as organic surfactants like polyethylene glycol, may drastically affect the seam formed between the two pillars which are being joined. Organic additives can also affect the electrical and mechanical properties of the electroless film in a variety of complex ways.[10, 13, 17] Thus, all experiments in this work were performed in an electroless bath formulated here.

The electroless bath used in this paper is described in Table 1. According to the mixed-potential theory, the reduction and oxidation reactions occur simultaneously on the copper surface, and their rates are independent of each other. The cathodic reactions occurring on the copper surface includes the reduction of the copper (II) ion, Equation 4, and the reduction of the copper (I) ion, Equation 5.[18]

[4]

[5]

A complexing agent, ethylenediaminetetraacetic acid (EDTA), is a used in a highly basic bath to prevent the formation of copper hydroxide. A stabilizing agent, potassium ferrocyanide, was also used in the bath in very low concentrations. The anodic reactions which take place on the copper surface include the hydrolysis of formaldehyde, Equation 6, dissociation of methylene glycol, Equation 7, dissociative adsorption Equation 8, charge transfer, Equation 9, and desorption of hydrogen, Equation 10.[18]

[6]

[7]

[8]

[9]

[10]

As noted previously, removal of adsorbed hydrogen from the copper surface is a critical factor in achieving an electroless bond with a low porosity, especially at high plating rates.[5] The open surface plating rate observed for this simplified bath was 10 μm/hr, and it was similar to that reported by Osborn et al.[5]

3.2 Polymer Collar Optical Characterization and Process Optimization

Photo-definable polymers with high contrast and high sensitivity are valuable because of their ability to form thick, high aspect ratio polymer structures. The polymer structures must also have high mechanical strength and excellent optical properties to be suitable as a polymer collar support and electroplating mold for all-copper interconnects.

The spin speed versus thickness curve in Figure 4 illustrates that thick Avatrel 8000P films above 100 μm can be obtained in a single coat. Avatrel 8000P samples were baked

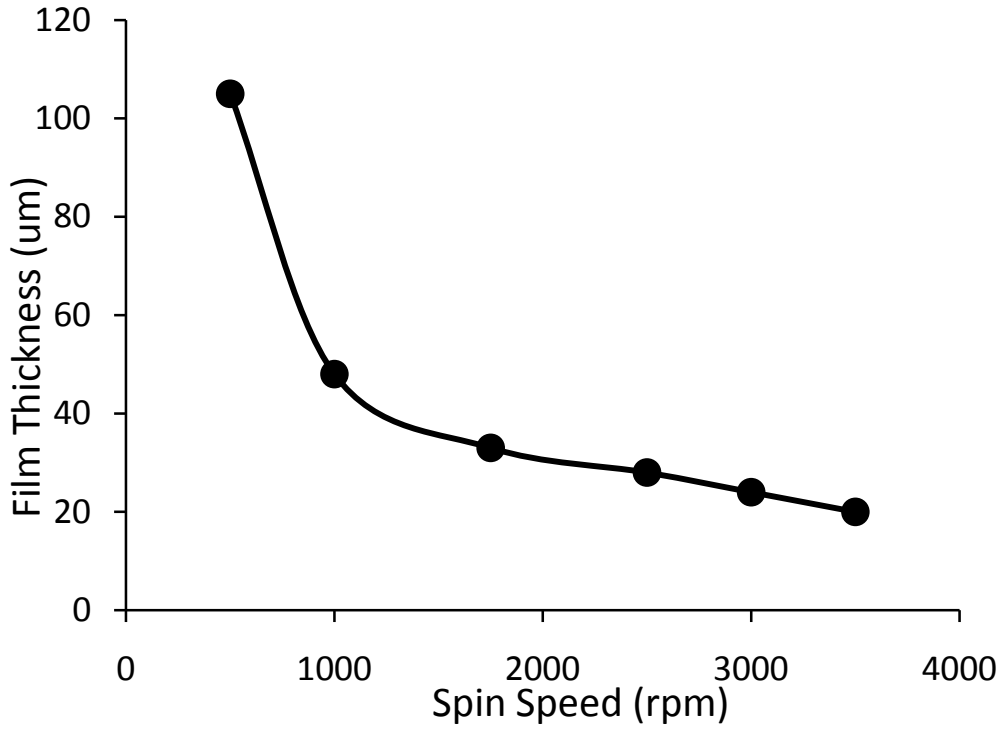

Figure 4. Avatrel 8000P spin speed versus thickness curve.

for 5 minutes before and after exposure at 100°C, whereas SU-8 requires longer processing times and temperature ramping steps for comparable film thicknesses. Avatrel 8000P was spun at 750 RPM, photo patterned with an exposure dose of 500 mJ/cm^2, and the resulting 70 μm features are shown in Figure 5. The lines in the SEM

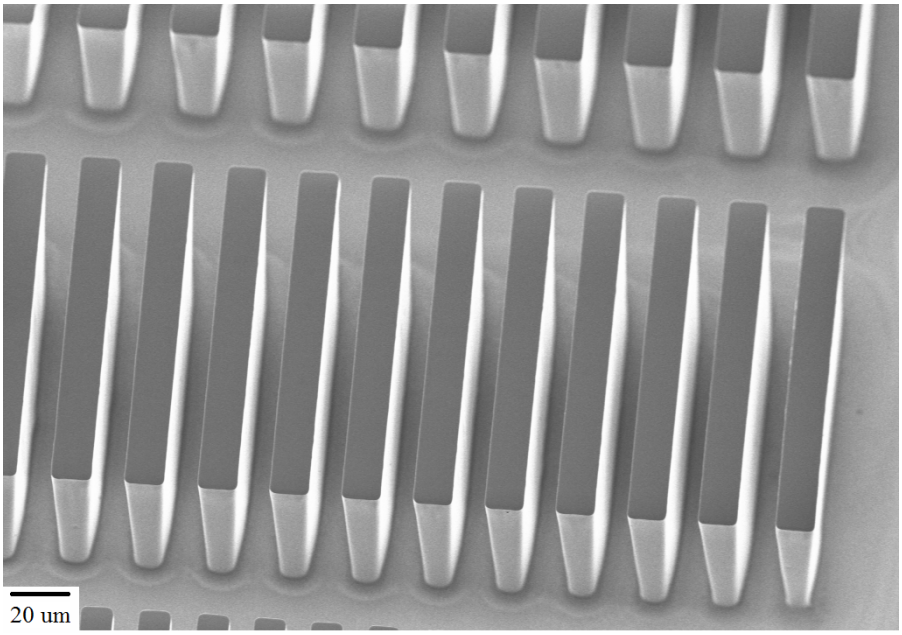

Figure 5. An S.E.M. image of 7:1 (height:width) Avatrel 8000P lines photo-patterned with an exposure dose of 500 mJ/cm^2.

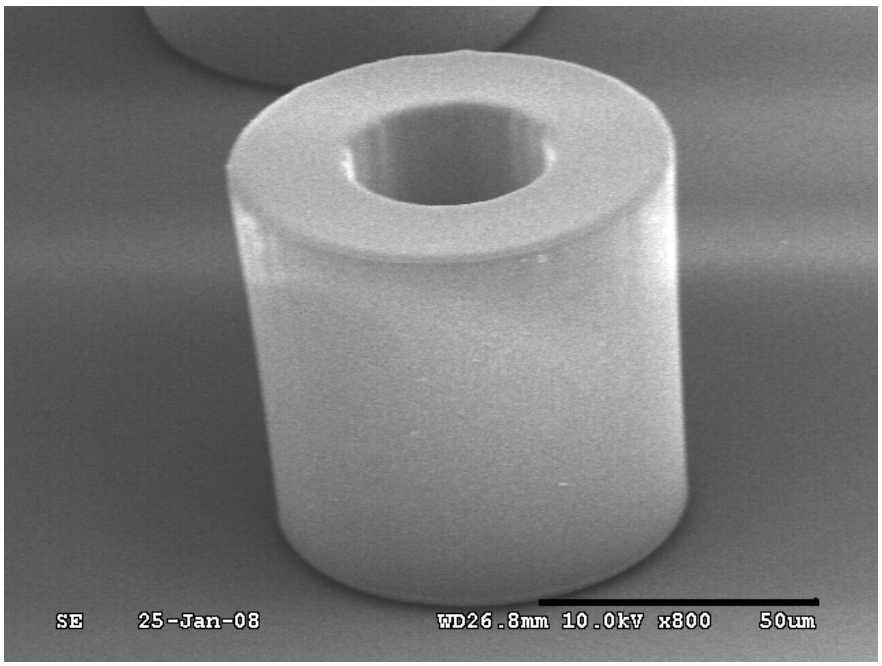

Figure 6. An S.E.M. image of 5:1 (height:width) Avatrel 8000P hollow core cylinder photo-patterned with an exposure dose of 500 mJ/cm^2.

image have a high aspect ratio of 7:1 (height:width) with smooth, straight side wall profiles. Avatrel 8000P was also evaluated for its ability to make complex shapes, and Figure 6 shows a hollow core cylindrical structure fabricated with the same processing conditions. The aspect ratio in Figure 6 is 5:1 (height:width) where the inside diameter of the core corresponds to the width dimension. The aspect ratio of the hollow structure is lower than the aspect ratio of the solid structure, because delamination occurred in cylinders with aspect ratios above 5:1. In high aspect ratio hollow structures, the transport of the developer in the core is slow compared to the transport of developer around the perimeter of the feature. As a result, hollow structures required longer develop times than solid features of comparable aspect ratios which caused delamination of features with aspect ratios above 5:1. The structures in Figure 5 have a slight non-vertical slope, but the hollow pillar in Figure 6 suggests that the taper is minimal. Sidewall slope may occur in thick, high aspect ratio structures due to UV absorbance in the film. Negative sloped sidewalls can be mitigated by using a filter to remove shorter wavelengths that are absorbed in the upper portion of the polymer and by optimizing the exposure dose and baking conditions to obtain uniform cross-link density throughout the film[27].

The contrast value of thick Avatrel 8000P films was measured to better understand the limitations of the material to pattern high aspect ratio features. Contrast is an important parameter for photoresists and is usually measured in thin films. Although contrast normally decreases with an increase in film thickness, the contrast value for Avatrel 8000P was high (γ=12.2). Figure 7 shows the contrast curve for a thick film of

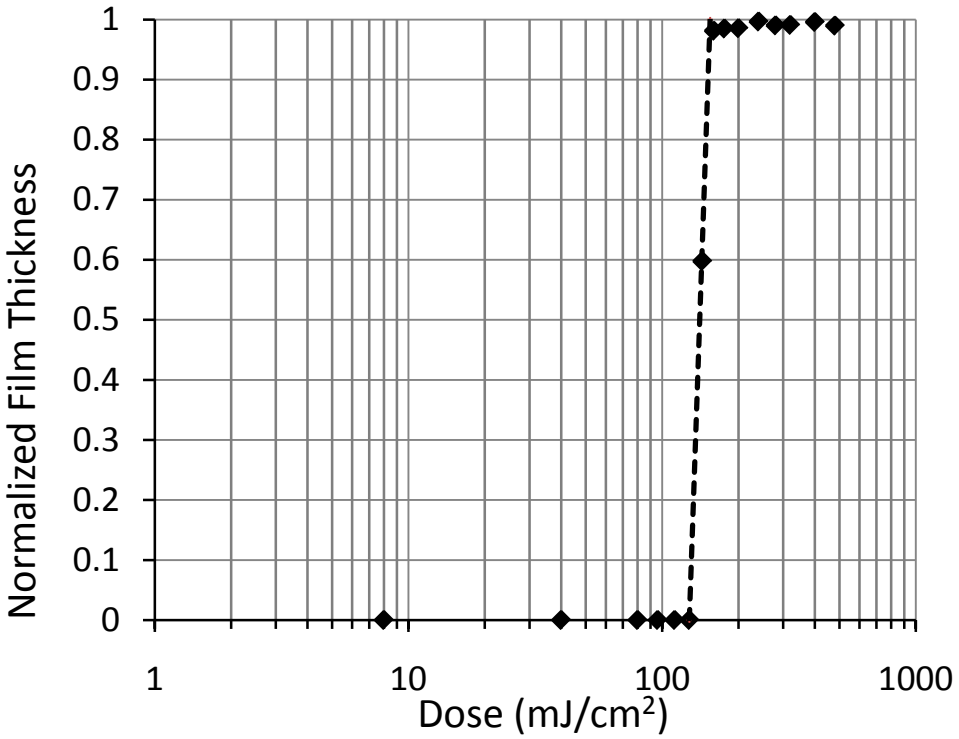

Figure 7. Contrast curve for thick Avatrel 8000P films obtained using front-side exposure ($\gamma = 12.2$).

Avatrel 8000P using front-side exposure, and a least squares method was used to fit the slope of the line from D_0 to D_{100} (Eqn. 1). Measuring contrast using front-side exposure is appropriate for processing applications, but the accuracy of the contrast is limited by the number of obtainable data points between D_0 and D_{100}. Contrast measurements are traditionally conducted in thin films where dose can be considered relatively constant through the film thickness. However, in thick films, the exposure dose at the top of a feature is higher than the dose at the bottom of a feature due to absorption of UV light within the film. Also, the cross-link density can effect the swelling and dissolution of the film Obtaining data points between D_0 and D_{100} is particulary difficult for negative-tone,

thick film polymers. For comparison, contrast measurements were conducted using front-side exposure for SU-8 and Avatrel 2000P as shown in Figure 8. In these figures, the films irradiated with doses near D_{100} suffer delamination due to poor substrate adhesion and high film stress. The contrast values are not reported due to the diffuclty in determining the exact value of D_{100} due to delamination. The sensitivity of SU-8 and Avatrel 2000P are 40 mJ/cm^2 and 176 mJ/cm^2, respectively.

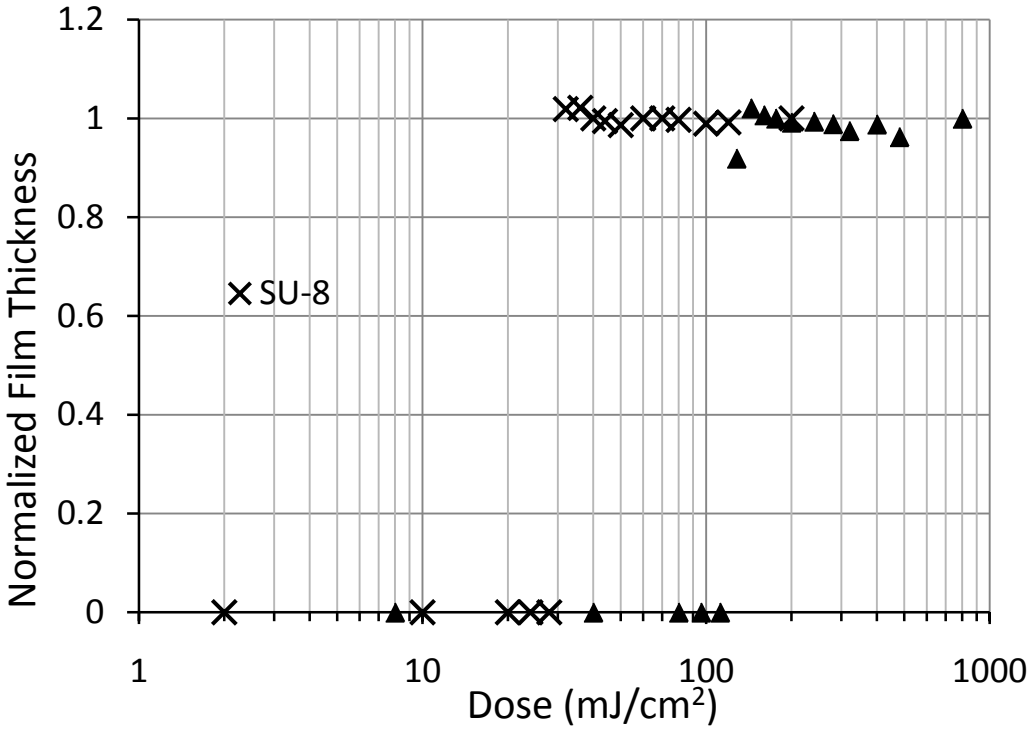

Figure 8. Contrast curve for thick Avatrel 2000P and SU-8 films obtained using front-side exposure.

A series of back-side exposures were performed to evaluate the impact of adhesion on the contrast values. Irradiating the polymer through a UV transparent substrate results in the highest exposure dose and highest level of cross-linking at the

polymer-substrate interface. Since the swelling and/or dissolution rate near the bottom of a feature was less than the top surface with back-side exposure, more data points could be collected between D_0 and D_{100}. Figure 9 shows the contrast curve obtained for Avatrel 8000P through back-side exposure and after curve fitting the contrast was found to be 9.04. The lower contrast value obtained from backside exposure is attributed to the shift in the D_0 and D_{100} doses. The shift of D_0 and D_{100} occurs because the level of cross-linking at the top and bottom of the film differ from the case of front-side exposure, resulting in different dissolution rates for the two exposure methods.

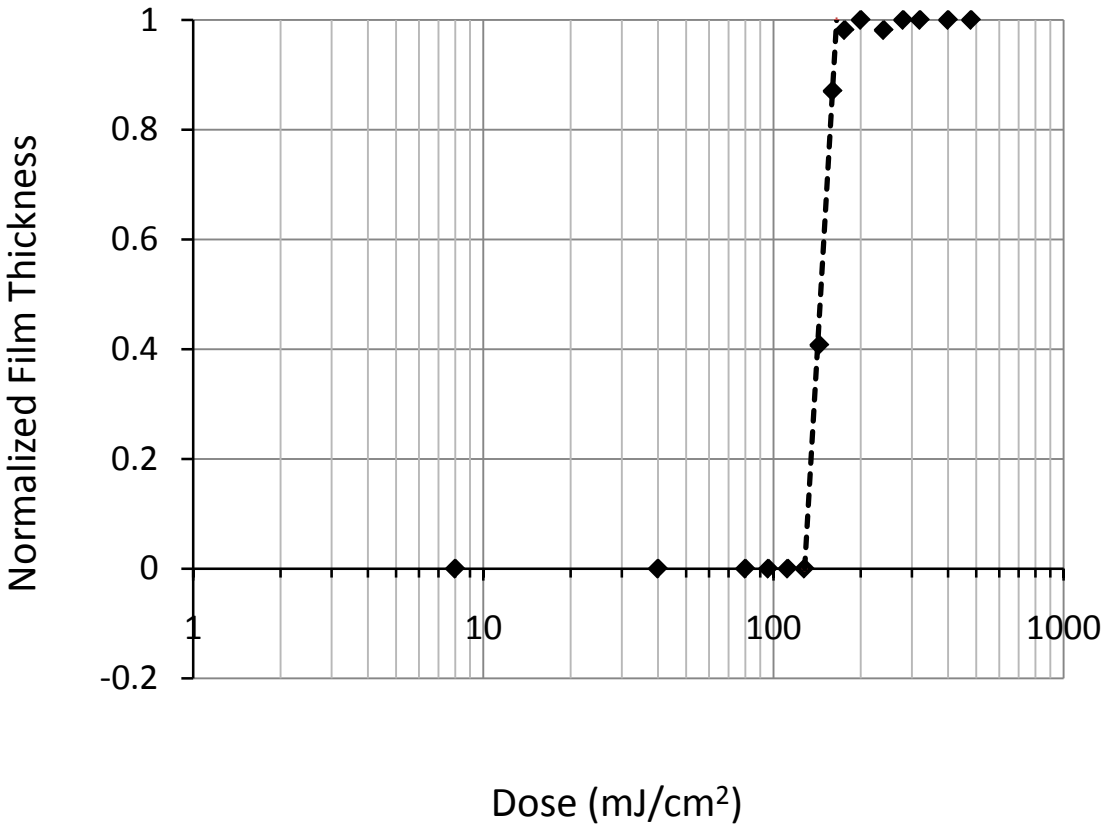

Figure 9. Contrast curve for thick Avatrel 8000P films obtained using back-side exposure ($\gamma = 9.04$).

As previously mentioned, the absorption coefficient of a photo-definable material impacts its resolution and ability to make high aspect ratio features in thick films. Eyre et al. have shown that if the optical absorption of a photo resist is too high, UV light will not penetrate a thick resist layer and therefore clean, sharp images cannot be generated[19]. The absorption coefficient of fully formulated Avatrel 8000P (i.e. with epoxy functionalized crosslinker, and photo-package) was measured after soft-bake, exposure, and post exposure bake. As shown in Figure 10, the absorption coefficient at 365 nm is 110 cm^{-1} after soft-bake and 94 cm^{-1} after post exposure bake. The decrease in absorption

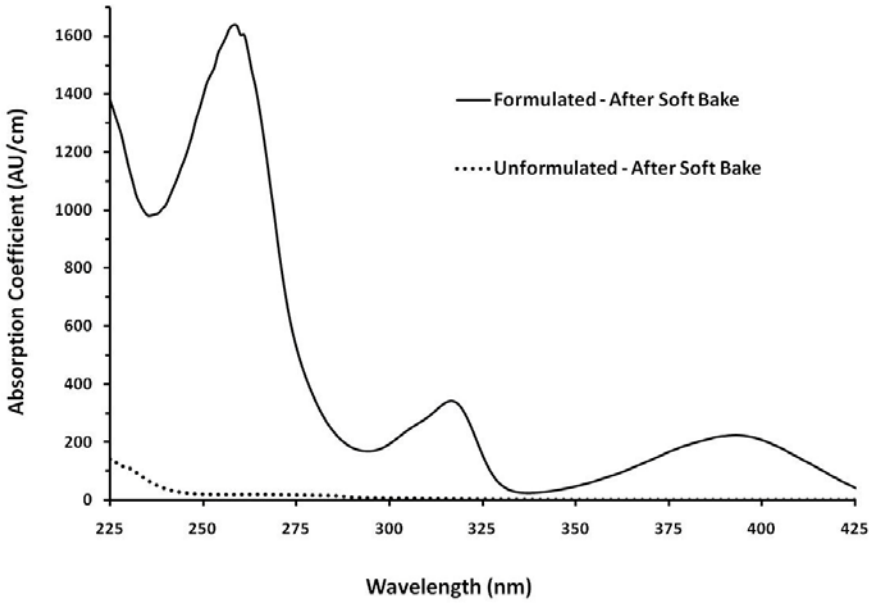

Figure 10. Changes in the absorption coefficient of fully formulated Avatrel 8000P and pure norbornene Avatrel 8000P from 225 nm – 425 nm.

coefficient is due to decomposition of the photo-catalyst after exposure, lowering the concentration of the absorbing species. To evaluate only the contribution of the norbornene copolymer, the absorption coefficient of the norbornene copolymer was

measured in propylene glycol monomethyl ether acetate (PGMEA). At the 365nm, the absorption coefficient is 0.25 cm^{-1}, indicating that the norbornene molecule absorbs a small amount of photons compared to the photo-package. Thus, the high aspect ratios of the patterned Avatrel 8000P films is a result of the high contrast values and low absorption coefficient.

CHAPTER 4

ELECTROLESS BONDING AND ANNEALING

4.1 Bonding over Large Gaps

To analyze the electroless copper bonding process and to demonstrate process dexterity, two samples with copper pads, instead of copper pillars, were electrolessly bonded over a standoff distance of 117.5 μm (± 2.6 μm, microsphere diameter error) for approximately 10 hours. A diagram of the pad-to-pad system is shown in Figure 2B. In this system, transport of the solution between the two chips is less restricted and simplified. Since a polymer mold is not necessary in this scenario, organic contamination of the bath is reduced.

As seen in Figure 11A, bonding does not always occur between areas of overlap between the two pads. A bond between pads of two aligned substrates is never noticed below 2 hours of plating time. In this time frame, the vertical and horizontal deposition rates are approximately equivalent resulting in 20 μm of deposited copper. At this point, no bonds have formed between any set of copper pads. After two hours of plating time, irregular growth of thin copper cylinders are noticed primarily in the vertical direction between the two pads. This growth of preferential grains on the electrolessly plated surface of the copper pads and an acceleration of the plating rate inside the narrow gap leads to copper bonds (thinner than the pads) between the two pads. The acceleration of the plating rate inside a narrow gap, as previously reported, has been achieved using a commercial copper electroless plating bath [3] and using electroless nickel [20]. These results show that the connection between the closely approaching surfaces during plating

occurred by electroless plating even without a surfactant or organic accelerator in the bath. Since bonding occurs in such a manner, bonding between two separate copper surfaces and the resulting bond yield is assumed to be strongly dependent on the distance between the copper surfaces.

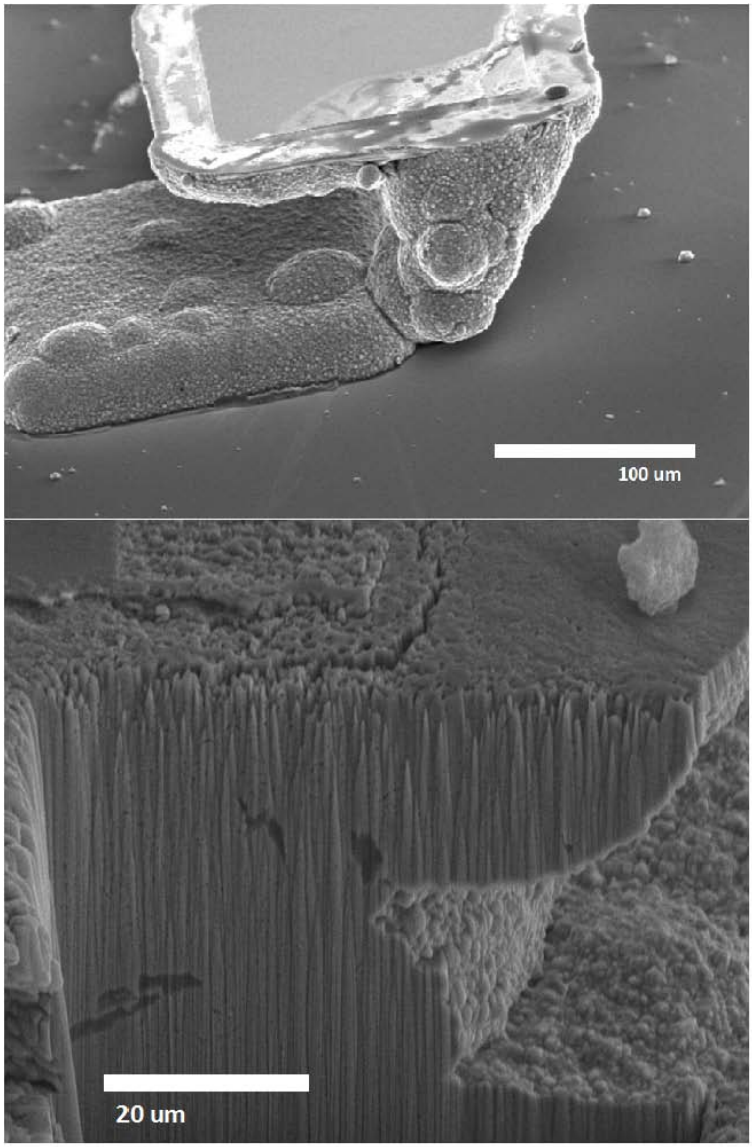

Figure 11. Two SEM images of (A) a bonded and sheared interconnect formed in a pad-to-pad system and (B) the cross-section (prepared by FIB) of a bonded and sheared interconnect formed in a pad-to-pad system.

The strength of bond between the two pads was strong enough that when sheared, the interconnect failed at the interface between the copper pad and substrate (Cr-Substrate interface) and not in the electroless joint. The average adhesion strength was calculated as the shear force divided by the contact area (i.e. area of the base of the pillar), and it was less than 13 MPa. The copper bond strength was in excess of this value. However, the electroless bond strength could not be determined for these samples because the failure point of the interconnects was not in the electroless joint. Osborn et al. have reported that annealing is essential to improve the bond strength between the two copper pillars.[3, 5] Low temperature annealing is desirable in order to minimize the thermal budget of the organic substrates (e.g. FR-4). We observed that even at 160°C, good bonding yield was observed with failure occurring at the Cr-Substrate interface rather than in the electroless joint. Furthermore, even without annealing, bonding between the two pads occurred and the bond withstood the shear force to rupture at the pillar-to-substrate metallization. These results suggested that the bonding of two copper pads could be obtained at anneal temperatures lower than 160°C.

Ion beam imaging after FIB milling of the bonded parts showed that the Cu structure is continuous (Fig. 11B). The bonding area within the electroless metal consisted of fine grains without the presence of seams (defined in Secion 4.3). In Fig. 11B, macroscale voids (defined in Section 4.3) were observed to occur randomly in the electroless bonded regions. The macroscale voids were very narrow and their length was on the scale of a few micrometers, so their existence is likely due to the nonplanarity obtained during electroplating (discussed further in Section 4.3).

4.2 Affect of Annealing on the Electroless Bond: Quantification

To examine the effect of annealing on the electroless copper bond formed between to copper pillars in a flip-chip configuration (Fig. 2A), quantification of the bond strength and examination of the bond (i.e. analysis of the grain structure and defects) were performed. Figure 12 shows a typical pillar-to-pillar bond formed. The structure was made by bringing together two silicon components, each with an electroplated copper pillar. The gap between the two pillars was filled with electroless copper, which joined together the components. Each of the two pillars in Fig. 12 has an electroplated copper core with electroless copper shell bonding the two structures together.

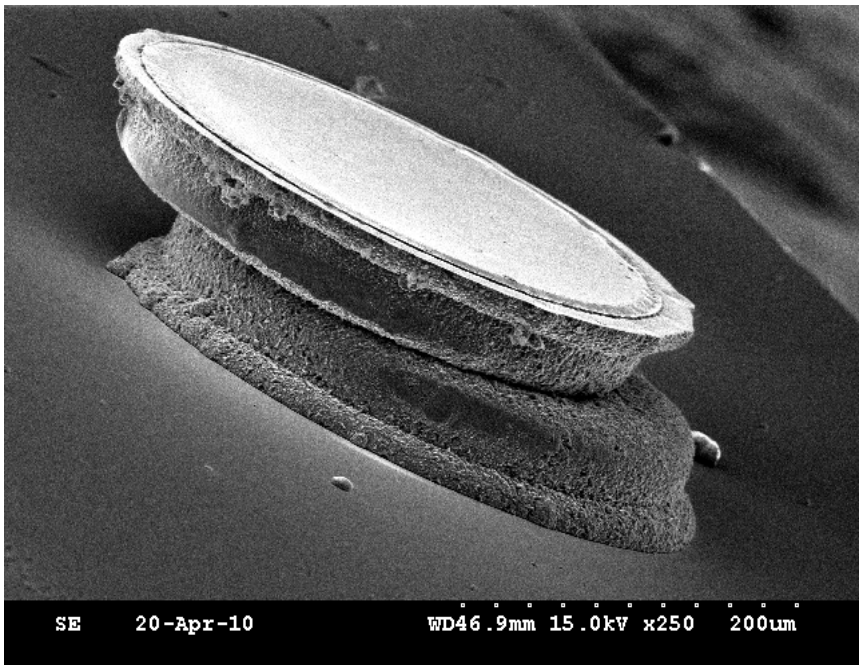

Figure 12. An SEM image of a delaminated (i.e. failed at the Cr-Substrate interface) interconnect.

Shear testing of the pillar-to-pillar bonds resulted in metal failure at one of two possible locations. Fracture occurred within the pillar-to-pillar, electroless copper bond, or adhesively at the pillar-to-silicon interface. Analyses of the shear tests are complicated because both types of failure occurred. The adhesion of the Cr/Cu layer to the silicon dioxide surface on the silicon wafer was excellent, especially with the added 250^{o}C anneal of the bond. Thus, parts which fail at the Cr/Cu-to-wafer interface show that the electroless copper joint is stronger than the surface adhesion. Some parts failed within the electroless copper joint, especially if the annealing of the electroless copper was inadequate or if the pillars on the two flip-chip aligned substrates were mis-aligned. Thus, isolating the strength of the electroless bond is difficult, since the electroless bond strength is generally stronger than the adhesion strength of the pillar to the substrate.

The strength of the electroless copper bond between pillars (i.e. bond strength) was quantified by bonding, annealing, and shear testing multiple all-copper pillars simultaneously. The bond strength measured here, as expressed in units of pressure, was obtained by measuring the shear force for dislodging one silicon substrate from the other, divided by the normalized interfacial area of the bond. The interfacial area is different for the two modes of failure (i.e. pilot-to-pillar failure or adhesive failure of the Cr/Cu-to-silicon joint) because the electroless plating may not have filled the entire regions between the two copper pillars (e.g. under-plated parts or misaligned pillars). For components which had both kinds of failure, the interfacial area used was the sum of two different types of areas: (i) adhesive delamination area (i.e. the area at the base of the pillar where the pillar failed), and (ii) bonded area (i.e. the area of the broken electroless bond at the joint between two electrolessly bonded pillars).

The test structure for bond strength, as shown in Fig. 2A, was used for pillar-to-pillar bonding. In Figure 13, the bond strength of the all-copper pillars is shown as a function of the anneal temperature (one hour anneal in each case). The total bonded area was the sum of the cross-sectional pillar area in the case of adhesive pillar to substrate fracture, or the pillar-to-pillar contact area for fractures that occurred within the electroless bond. Misalignment of the two parts often caused the pillar-to-pillar bonded area to be less than the cross-sectional area of the pillars. The overall trend in bond strength is increasing with higher anneal temperature. The as-plated samples showed considerable bond strength, approximately 8 MPa.

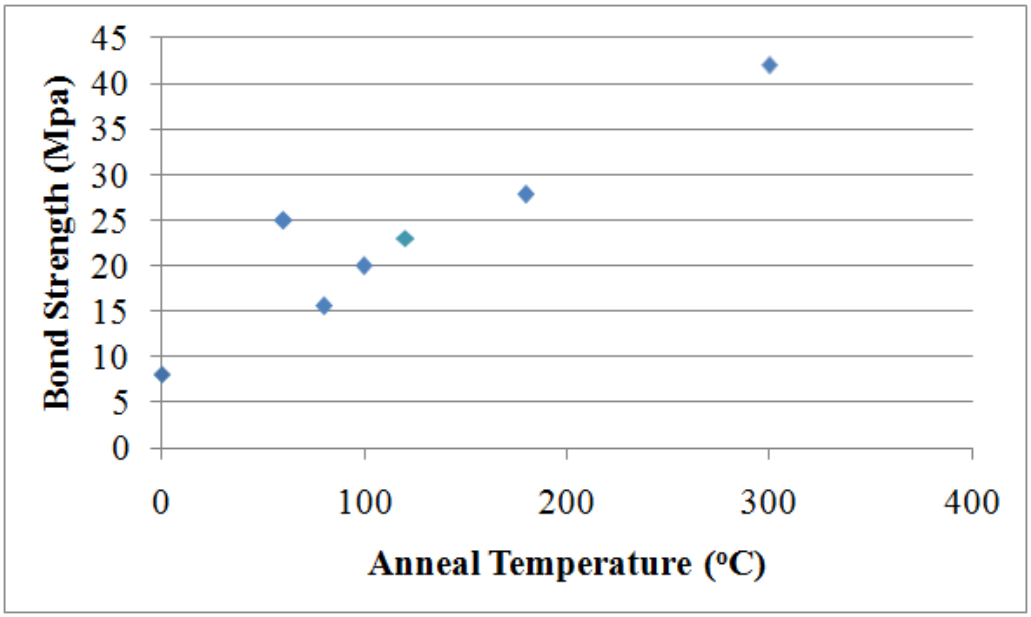

Figure 13. The average electroless bonding strength as a function of anneal temperature.

The fraction of the pillars failing at the pillar-to-substrate interface is shown in Figure 13. Since more than 80 percent of the pillars failed adhesively at the base of the pillar when annealed at 80°C to 120°C (Figure 14), the cross-sectional area of the pillar was taken as the bond area for those pillar, and not the pillar-to-pillar overlap area to calculate the bond strength. The pillar-to-pillar overlap area, for those pillars which broke in the electroless copper region was typically less than 50% of the cross-sectional area of the pillar due to chip misalignment. The values of bond strength are comparable to the bond strength of a solder balls (100 µm diameter), which have been reported to be 36 MPa.[21]

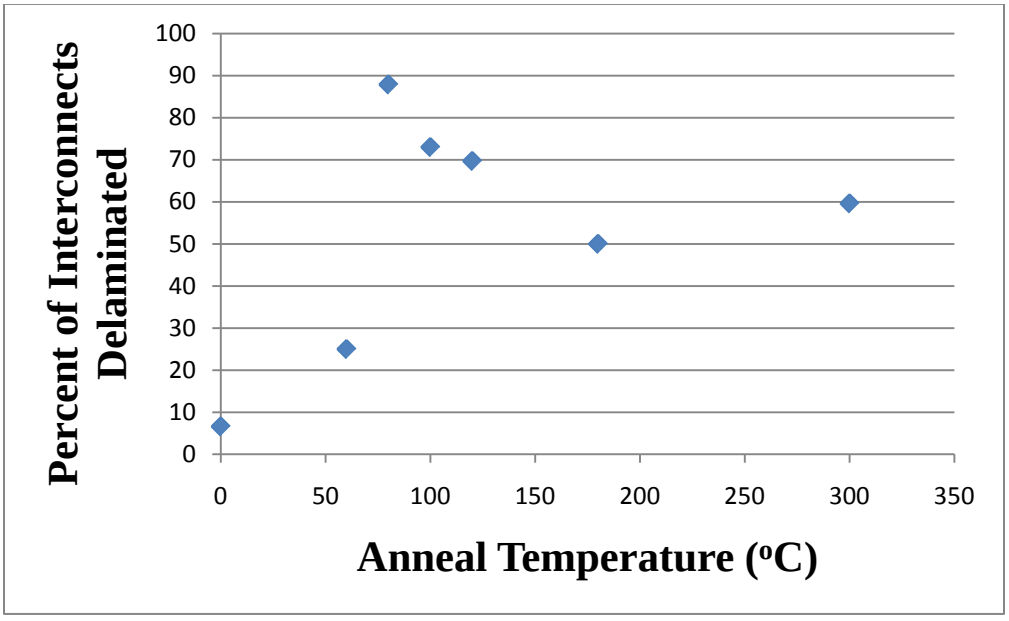

Figure 14. The percentage of all-copper interconnects which failed at the base as a function of anneal temperature.

4.3 Affect of Annealing on the Electroless Bond: Qualification

To obtain a better understanding of the electroless bond formed, the bond quality was analyzed by measuring the grain size and type of defects in the electroless copper region. Cross-sections were prepared by focus ion beam sectioning followed by examination in a scanning electron microscope. Cross-sections of the electroless bond on electroplated pillars are shown in Figure 15 for samples annealed at different temperatures ranging from no-anneal (left image in Fig. 5) to a sample annealed at 300^{o}C (right side of Fig. 15.) In each image, a cross-section of two aligned and bonded pillars is shown. A diagram of the cross-sectional structure is shown in Figure 16 for clarity. In each image in Fig. 15, the electroplated grains (average size, 5-10 μm) of the copper pillar are on average larger than those in the electroless copper region bridging the two pillars.

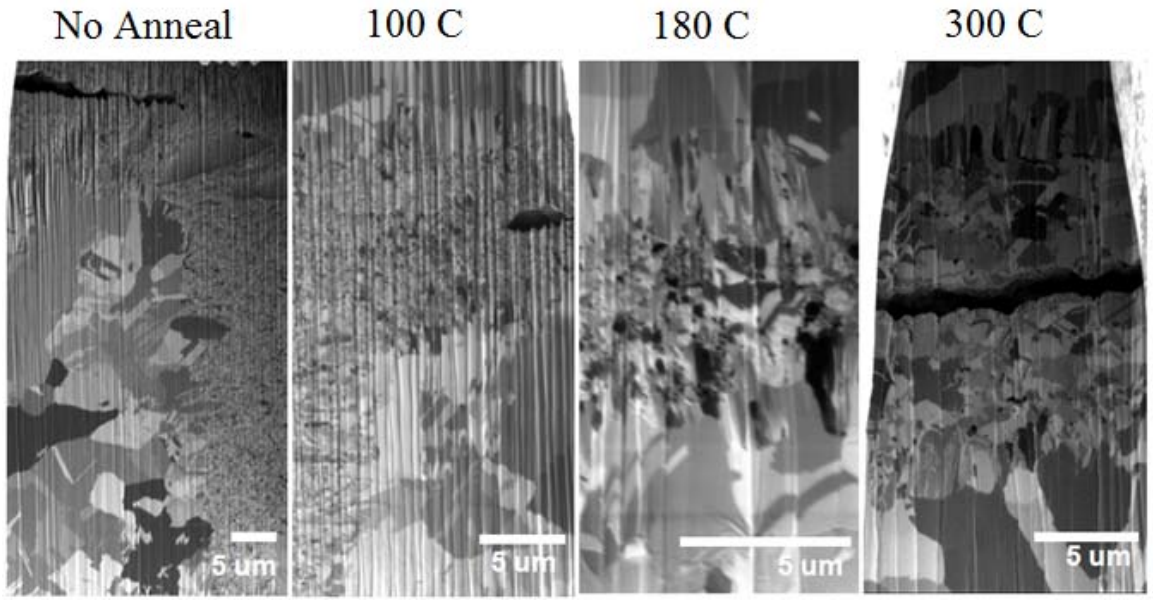

Figure 15. FIB/SEM images of cross-sections of the electroless bonding regions of samples which were (from left to right) not annealed, annealed at 100^{o}C, annealed at 180^{o}C, and annealed at 300^{o}C.

Electroplated copper often has large grains, especially after annealing at 250^{o}C, which occurred before the electroless bonding. Compared to the electroplated pillars, the electroless plated regions have a smaller grain size and can easily be seen. The cause of the smaller electroless grains is due to suppression of epitaxial growth on the existing copper grains and continuous nucleation in the electroless bath caused by adsorption of complexing agents, formaldehyde oxidation byproducts, and surface adsorbed hydrogen. Fig. 15 also shows that the electroless copper does not anneal to form the same size grains as the electroplated copper. The average electroless grain size was less than or equal to 100 nm in the images of the samples not annealed and annealed at 100^{o}C (Fig. 15), and the difference in electroless grain sizes between the two images is virtually indistinguishable. Thus, the lack of grain growth at temperatures below 100^{o}C did not promote pillar-to-pillar bonding. However, the removal of entrapped hydrogen and other impurities from the electroless bond and subsequent ductility increase likely assisted in improving the bond strength, as suggested previously.[17, 22] In the image of the sample annealed at 180^{o}C in Fig. 15, the average electroless grain size increased to 500-700 nm. As anticipated, the largest grain sizes are observed for samples annealed at 300^{o}C, where the average electroless grain size was 1-2 μm.

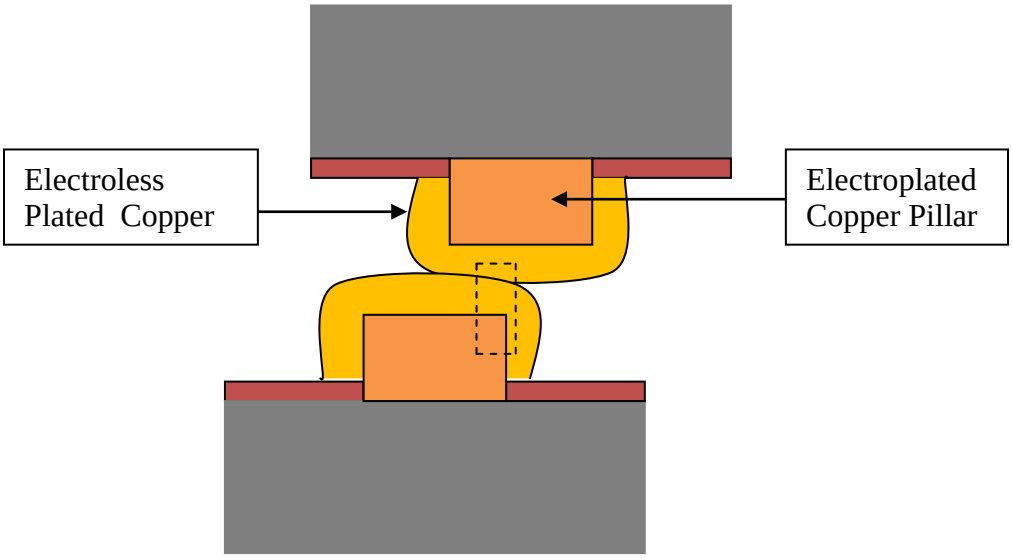

Figure 16. A diagram of the cross-sectioned area (dotted line) on a bonded all-copper interconnect which was prepared by FIB.

Also apparent in Fig. 15 are two types of defects at the interface between to electroless copper on each of the two pillars: (i) voids (i.e. large gaps between copper surfaces or copper surfaces not in electrical contact), and (ii) seams (i.e. copper surfaces in electrical contact but with a fine boundary between the two electroless plated regions). Entrapped voids (scaling 2-3 μm in height and tens of micrometers in length) are noticeable. Voids, such as these, may be caused by the sealing of the gap through electroless plating between pillars which were rough and nonplanar. Sharp ridges and valleys, with a height difference of 3 to 5 μm existed on the surface of the pillars prior to electroless plating. These macroscale voids were not filled by electroless plating and were not removed during the annealing process. Grain growth during annealing eliminated grain boundaries and removed the ‘seam’ (second type of defect between

electrolessly plated pillars) through grain merging. To avoid the need for high temperature and pressure, the elimination of larger voids should be addressed at the pillar electroplating stage by making smoother pillars.

The gap between the two pillars to be filled by electroless copper, and diameter of the pillars, along with the aspect ratio (standoff distance between two copper surfaces divided by the copper pillar diameter) are important parameters in creating void-free bonds. Transport limitations of plating reactants and removal of plating by-products inside the gap between the pillars to be bonded can lead to edge bonding and subsequent macroscale void entrapment near the center of the electroless bond. Creating a pillar with minimal surface roughness and a domed top surface may allow for a void-free bond to be created with a minimal standoff distance between aligned pillars.

A seam was created at the point where the electroless plating front of two copper pillars merge. The presence of a seam suggests intimate, electrical contact between two copper surfaces and a point of mechanical weakness apparent from the disparate grain boundaries, as was shown previously.[3, 5] The surface condition and presence of adsorbed organic surfactants, such as polyethylene glycol, appears to promote a more dramatic seam and requires a higher temperature anneal to remove the seam. In Fig. 15, the seam is evident in the image of the unannealed sample. It is difficult to find any seam for samples annealed at 100^{o}C. Thus, it appears that modest temperature anneal (e.g. 100^{o}C) is adequate to remove seams for the surfactant-free surfaces here, in comparison to the higher temperature anneal required with surfactants were present.[5] Since a natural point of crack initiation and failure is at a grain boundary, a seam-free electroless bond implies a more mechanically robust structure.

Micro-scale voids were also found in the electrolessly plated copper structure, as shown in Fig. 15. Microscale voids are can be caused by hydrogen bubble entrapment during electroless plating. In some cases, hydrogen bubble entrapment can block the formation of an electroless bond between two copper surfaces. Organic surfactants, such as polyethylene glycol and be used to remove adsorbed hydrogen from the electroless copper surface.[5] In addition, high plating rate are desired in order to decrease plating time, which could lead to higher hydrogen entrapment.

CHAPTER 5

CONCLUSION

Avatrel 8000P's excellent photo-definition properties and mechanical strength make it an ideal polymer collar material. Avatrel 8000P is a high contrast, I-line sensitive mixture that can be developed in traditional aqueous-base developers. The great photolithographical performance of this photopolymer can be partly contributed to the minimal amount of light absorbed by the base norbornene polymer. The processing conditions noted in this work are an optimized version, which have been shown to give superior photolithographical performance. The simple baking procedures make Avatrel 8000P easier to process than SU-8. The ability to develop Avatrel 8000P in aqueous base can reduce chemical waste. As shown by SEM images, high fidelity structures with aspect ratios of 7:1 can be fabricated in thick films with vertical sidewalls.

Bonding between two copper surfaces over various gap sizes was achieved by electroless deposition without the addition of surfactants or inhibitors in the bath. The effect of anneal temperature on the electroless bond formed was analyzed. The electroless bond strength increased with anneal temperature. However, the bond strength estimation for samples annealed at 80^{o}C to 120^{o}C is a minimum value due to the failure location of most of the pillars and the resulting area used in the calculation of bond strength. Grain growth from copper recrystallization and removal of small defects improve the bond strength. Large voids at the interface of the two pillars were related to rough starting surfaces for the electroplated pillars.

REFERENCES

1. Moore, G., *Cramming more components onto integrated circuits.* Proceedings of the IEEE, 1998. **86**(1): p. 82-85.
2. Tie Wang, F.T., Louis Foo, Vivek Dutta, *Studies on A Novel Flip-Chip Interconnect Structure - Pillar Bump*, in *Electronic Components and Technology Conference*. 2001.
3. Osborn, T., et al., *All-Copper Chip-to-Substrate Interconnects Part I. Fabrication and Characterization.* Journal of the Electrochemical Society, 2008. **155**: p. D308.
4. He, A., et al., *All-Copper Chip-to-Substrate Interconnects Part II. Modeling and Design.* Journal of the Electrochemical Society, 2008. **155**: p. D314.
5. Osborn, T., N. Galiba, and P. Kohl, *Electroless Copper Deposition with PEG Suppression for All-Copper Flip-Chip Connections.* Journal of The Electrochemical Society, 2009. **156**: p. D226.
6. Chen, K., et al., *Copper bonded layers analysis and effects of copper surface conditions on bonding quality for three-dimensional integration.* Journal of Electronic Materials, 2005. **34**(12): p. 1464-1467.
7. Kim, T., et al., *Room temperature Cu–Cu direct bonding using surface activated bonding method.* Journal of Vacuum Science & Technology A: Vacuum, Surfaces, and Films, 2003. **21**: p. 449.
8. Osborn, T., C. Hunter Lightsey, and P. Kohl, *Low-k compatible all-copper flip-chip connections.* Microelectronic Engineering, 2009. **86**(3): p. 379-386.
9. Lee, C., S. Cho, and J. Kim, *Electroless Cu bottom-up filling using 3-N, N-dimethylaminodithiocarbamoyl-1-propanesulfonic acid.* Electrochemical and Solid-State Letters, 2005. **8**: p. J27.
10. Koo, H. and J. Kim, *Effects of Stabilizing Agents on Film Properties in Ag Electroless Plating.* Journal of The Electrochemical Society, 2008. **155**: p. D176.
11. Bogush, V., et al., *Material properties of very thin electroless silver-tungsten films.* Thin Solid Films, 2003. **426**(1-2): p. 288-295.
12. Rajarathinam, V., et al., *Aqueous-Develop, Photosensitive Polynorbornene Dielectric: Properties and Characterization.* Journal of Electronic Materials, 2009. **38**(6): p. 778-786.
13. Stangl, M., et al., *Investigation of organic impurities adsorbed on and incorporated into electroplated copper layers.* Applied Surface Science, 2005. **252**(1): p. 158-161.
14. Bai, Y.Q., et al., *Photosensitive polynorbornene based dielectric. I. Structure-property relationships.* Journal of Applied Polymer Science, 2004. **91**(5): p. 3023-3030.
15. Bai, Y.Q., et al., *Photosensitive polynorbornene based dielectric. II. Sensitivity and spatial resolution.* Journal of Applied Polymer Science, 2004. **91**(5): p. 3031-3039.
16. ; Available from: http://www.microchem.com/products/su_eight.htm.

17. Okinaka, Y. and H. Straschil, *The effect of inclusions on the ductility of electroless copper deposits.* Journal of The Electrochemical Society, 1986. **133**: p. 2608.
18. Schlesinger, M. and M. Paunovic, *Modern electroplating*. 2000: Wiley New York, NY.
19. Eyre B, C.J.a.W.D., in *11th IEEE Micro. Elec. Mech. Sys.* 1995: Chicago, USA. p. 218.
20. Yokoshima, T., et al., *Anisotropic Deposition of Localized Electroless Nickel for Preferential Bridge Connection.* Journal of The Electrochemical Society, 2010. **157**: p. D65.
21. Lau, J.H., Pao, Y.H. , *Solder Joint Reliability of BGA, CSP, Flip Chip, and Fine Pitch SMT Assemblies*. 1997, NY: McGraw-Hill.
22. Nakahara, S. and Y. Okinaka, *Microstructure and ductility of electroless copper deposits.* Acta Metallurgica, 1983. **31**(5): p. 713-724.